Desalination and Water Treatment
www.deswater.com

doi: 10.1080/19443994.2016.1174743

57 (2016) 27269–27278
December

Taylor & Francis
Taylor & Francis Group

Basic Blue 41 removal by microwave hydrothermal reactor reduced graphene oxide

Salimeh Kimiagar[a,*], Nasim Rashidi[a], Bartłomiej S. Witkowski[b]

[a]*Nano Research Lab, Department of Physic, Islamic Azad University, Central Tehran Branch (IAUCTB), Tehran 14676-6831, Iran, Tel. +98 21 88372704; Fax: +98 21 88385777; emails: kimia@khayam.ut.ac.ir (S. Kimiagar), nasim.rashidi70@gmail.com (N. Rashidi)*

[b]*Institute of Physics, Polish Academy of Sciences, al. Lotników 32/46, 02-668 Warsaw, Poland, Tel. +48 22 116 2663; Fax: +48 22 843 09; email: bwitkow@ifpan.edu.pl*

Received 2 December 2015; Accepted 13 March 2016

ABSTRACT

Graphene oxide was prepared using Hummer method and reduced by microwave hydrothermal reactor. The characteristics of RGO nanosheets were determined with EDAX, X-ray diffraction, FTIR, scanning electron microscopy, and AFM. RGO nanosheets have been utilized as the adsorbent for the removal of Basic Blue 41 (BB41) dye from an aqueous solution at room temperature (298˚K) as an appropriate innovative and low-cost adsorbent. The effect of pH, adsorbent dose, contact time, and initial dye concentration on adsorption was studied. The results indicated that RGO can be employed as a low-cost alternative compared to other commercial adsorbents in the removal of dyes from wastewater. The maximum adsorption capacity was at pH 9 and 0.05 g of RGO adsorbent dose. It was shown the rapid adsorption of BB41 in the first 180 min contact time. The BB41 removal percentage decreased as the initial dye concentration increased. The experimental data were analyzed by Langmuir and Freundlich adsorption isotherms. According to the determined coefficients, the Langmuir model was fitted better than the Freundlich model. The results indicated that RGO could be employed as an excellent sorbent for removal of BB41 dye from an aqueous solution.

Keywords: Graphene; Basic Blue 41; Microwave hydrothermal reactor; Removal

1. Introduction

Wide use of dyes in industries such as textiles, dyeing, electroplating, printing, and tanneries leads to large amounts of dye-containing wastewater to be discharged into the environment [1]. The complex aromatic structures of dyes make them more difficult to degrade [2]. Dyes are harmful to flora and fauna, and their products have a mutagenic or carcinogenic influence and toxic to human health [3]. Consequently, much attention should be paid to treat dyes before discharge. The Basic Blue 41 (BB41) has wide applications in industries. Thus, the removal of BB41 from industrial effluents has become one of the major environmental concerns.

Several wastewater treatment methods have been used for the treatment of colored effluent in recent years. Those methods include chemical oxidation [4], filtration [5], biological treatment [6], and adsorption

*Corresponding author.

[7,8]. Among the mentioned methods, adsorption processes are attractive because of their high efficiency, low cost, with good final quality, and no harmful substance production. Carbonaceous materials such as activated carbon [9], carbon nanotubes [10], and their composites are the most commonly used dye adsorbents [11].

Graphene has attracted great attention for its remarkable electronic and thermal conductivity, large specific surface area, high mobility of charge carriers, excellent chemical stability, and mechanical strength due to its unique structure made of sp^2 carbon atoms tightly packed into a honeycomb lattice [12]. GO-derived materials include chemically functionalized [13] or reduced graphene oxide sheets [14], assembled paper-like forms [15,16], and graphene-based composites [17]. Due to the attached oxygen functional groups, GO is electrically insulating and different reduction methods have been developed to repair its electrical conductivity. Chemical reduction using agents such as hydrazine or dimethyl hydrazine [18], hydroquinone [19], and $NaBH_4$ [20] have been used to reduce GO. As a convenient and rapid method, microwave hydrothermal reactor (MHR) has been used to reduce GO (RGO). This method can reduce GO sheets in a short time and moderate temperature. Recently, graphene and graphene oxide were used as adsorbents to remove methyl orange [21], naphthalene [22], fluoride [23], and Cu^{2+} from aqueous solutions, and showed high adsorption capacities and fast adsorption rates.

In this study, BB41 azo dye was selected to study as a typical adsorbate and used RGO nanosheets as an adsorbent to remove BB41 from aqueous solution. The influences of parameters such as pH, contact time, initial BB41 concentration, and RGO dosage on the adsorption capacity have been investigated in detail to increase our understanding of the dye adsorption properties of graphene.

2. Experimental details

2.1. Preparation of GO and RGO

GO was prepared using the modified Hummers method [24]. At first step, 9:1 mixture of concentrated H_2SO_4/H_3PO_4 (180:20 mL) was added to a mixture of 3.0 g of graphite flakes (Sigma-Aldrich, cat #332461, 150 μm lateral dimensions) and 9.0 g of $KMnO_4$. Although temperature of the exothermic reaction was 40–45˚C, the mixture was heated to 55˚C and stirred for 12 h. The reaction was cooled and poured onto ice (400 mL) followed by addition of H_2O_2 (3 ml) until the color changed to brilliant yellow. The solution was centrifuged at 6,000 rpm for 6 h to eliminate the supernatants and washed with 200 ml of 30% HCl, 200 ml of 70% ethanol aqueous solution, and 200 ml of deionized water (2×). Each washing process was completed by centrifuging at 6,000 rpm for 30 min, and removing the supernatants. The obtained materials were exfoliated under sonication for about 3 h then the sonicated aqueous suspensions were centrifuged at 6,000 rpm for 4 h and the supernatants were removed (Fig. 1). The obtained materials were coagulated with 100 mL of de-ethyl ether and filtered using a polytetrafluoroethylene membrane (PTFE-0.22 μm pore size). The filtered powder was dried in vacuum-oven at 65˚C and 35 mm Hg overnight. The material was dissolved in 70 ml of distillate water. The solution was placed in the reactor (PTFE vessel of MHR Ertec) and was heated up to 250˚C at 40 atmospheres pressure for 2 h. These conditions were figured out in our previous study [25]. Applying MHR ensures the uniformity of temperature distribution. After the process, it was cooled down to room temperature. The resulting solution was filtered through the tissue. The structure of the GO and RGO samples characterized using X-ray diffraction (XRD). Fourier transform-infrared spectroscopy (FT-IR) was applied to investigate reduction of GO. The morphology and structure of GO and RGO nanosheets were investigated through scanning electron microscopy (SEM). AFM analysis confirmed existence of few-layer RGO nanosheets.

2.2. Batch adsorption experiments

Adsorption experiments were carried out at room temperature to study the effects of important parameters such as pH, contact time, initial BB41 concentration, and RGO dosage under the aspects of

Fig. 1. GO sample.

adsorption isotherms. BB41 was purchased from the Ciba chemical company (C.I. Basic Blue 41, chemical formula: $C_{19}H_{26}N_3O_6S_2$, MW: 456 g/mol, λ_{max} = 609 nm) and used without further purification. The structural form of dye is given in Fig. 2. The concentrations of BB41 solution before and after adsorption were estimated by measuring absorbance at 609 nm with help of UV–vis spectrophotometer (Perkin–Elmer UV–vis spectrometer).

A stock solution of BB41 (1,000 mg/L) was prepared and further diluted to the required concentrations before used. The adsorption experiments were conducted in 250-mL conical flasks with 100 mL of standard solutions and equilibrated in a temperature-controlled water bath shaker (SHZ-82A) at room temperature (298°K). After adsorption equilibrium, the concentration of BB41 in the solution was measured using a UV–vis spectrophotometer. The amount of dye adsorbed onto RGO, q_e (mg/g), was calculated according to the following equation:

$$q_e = \frac{(C_0 - C_e)V}{M} \quad (1)$$

where C_0 and C_e are the initial and equilibrium concentrations of BB41 in solution (mg/L), respectively, V is the volume of solution (L), and M is the mass of adsorbent (g).

The removal percentage of dye is defined as the ratio of difference in dye concentration before and after adsorption ($C_0 - C_e$) to the initial concentration of the dye (C_0) and was calculated using equation:

$$R\ \% = \frac{(C_0 - C_e) \times 100}{C_0} \quad (2)$$

The effect of initial pH on the adsorption of BB41 was studied in a pH range of 3.0–11.0 using 100 mL of solutions with 25 mg/L BB41concentration which were mixed with 0.005 g of RGO. The pH of the BB41 concentration was adjusted to the required pH value by adding 0.1 M NaOH or HCl. The pH of solution was measured with a Hanna pH meter using a combined glass electrode (Model HI 9025C, Singapore).

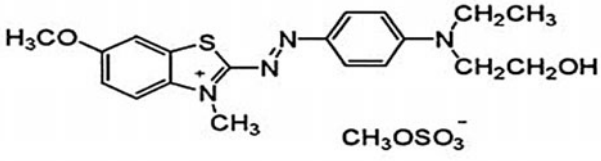

Fig. 2. The structure of BB41 dye.

The influence of graphene dose on the adsorption of BB41 was studied by agitating 100 mL of 50 and 75 mg/L solutions of BB41 with different dosages of graphene (0.003–0.09 g).

The result of contact time variation (0–300 min) on the adsorption of BB41 was studied by adding 0.05 g of adsorbents into 100 ml of 50 and 75 mg/L (BB41) solutions at room temperature. The initial BB41 concentration used in this study was 25–125 mg/L. At a preset time intervals, samples of these solutions were centrifuged (8,000 rpm) and filtered. The concentrations of BB41 solution before and after adsorption were estimated by measuring absorbance at 609 nm with help of UV–vis spectrophotometer.

3. Result and discussion

3.1. Characterization of RGO

The EDAX of the GO and RGO nanosheets as shown in the Figs. 3 and 4 confirms that carbon has increased in RGO sample and oxygen has decreased. The ratio of the elements present is in the required stoichiometric ratio is given in the table of the figures.

XRD patterns of GO and RGO nanosheets are presented in Fig. 5. The characteristic peak (0 0 2) of graphite at $2\theta = 26.6^\circ$ decreased after oxidation. In comparison to the natural graphite, a very wide peak is observed for GO and RGO, and it clearly indicates the damage of the regular crystalline of graphite pattern during the oxidation. The broad peak centered at $2\theta = 24.4^\circ$ in the XRD pattern of the RGO sample confirmed a random packing of graphene nanosheets in the RGO suggesting that the re-aggregation of RGO can be greatly limited [26]. The strong peak at $2\theta = 8.6^\circ$ is attributed to the (0 0 1) diffraction peak of RGO with interlayer spacing of about 0.84 nm which is significantly larger than that of graphite (0.334 nm, JCPDS No. 75-1621) [27]. The broadening and shift of the characteristic diffraction peak of graphite from 26.6° to 24.4° is due to the short-range order in stacked stacks [28]. These results indicating that GO has been successfully reduced to graphene nanosheets.

Fig. 6 shows the FT-IR spectra of GO and RGO. The main absorption peaks of oxygen-containing functional groups, including O–H at 3,340 cm^{-1}, C=O at 1,650 cm^{-1} and C–O 1,044 cm^{-1} consistent with the previous reports [13,25], are entirely vanished representing great effective deoxygenating of GO nanosheets via using MHR. Clearly, in this method GO was reduced completely without showing significant oxygen groups from 4,000 to 500 cm^{-1}.

Fig. 7 presents the SEM images of the GO nanosheets. These single or few-layer GO nanosheets

Element Line	Weight %	Weight % Error	Atom %	Atom % Error
C K	34.9	+/- 0.2	45.2	+/- 0.3
O K	49.3	+/- 1.0	47.9	+/- 0.9
Al K	0.8	+/- 0.0	0.5	+/- 0.0
Si K	1.4	+/- 0.0	0.8	+/- 0.0
Si L	—	—	—	—
P K	1.1	+/- 0.0	0.5	+/- 0.0
P L	—	—	—	—
S K	6.4	+/- 0.1	3.1	+/- 0.0
S L	—	—	—	—
Cl K	1.7	+/- 0.0	0.7	+/- 0.0
Cl L	—	—	—	—
K K	0.6	+/- 0.0	0.2	+/- 0.0
K L	—	—	—	—
Cr K	0.3	+/- 0.1	0.1	+/- 0.0
Cr L	—	—	—	—
Mn K	1.3	+/- 0.1	0.4	+/- 0.0
Mn L	—	—	—	—
Fe K	2.2	+/- 0.1	0.6	+/- 0.0
Fe L	—	—	—	—
Total	100.0		100.0	

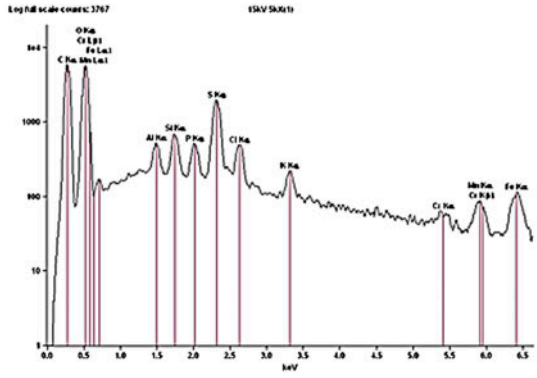

Fig. 3. Energy-dispersive spectra (EDX) of GO.

Element Line	Weight %	Weight % Error	Atom %	Atom % Error
C K	63.8	+/- 0.3	72.0	+/- 0.4
O K	29.5	+/- 0.5	25.0	+/- 0.4
Al K	2.1	+/- 0.0	1.1	+/- 0.0
Si K	3.1	+/- 0.1	1.5	+/- 0.0
Si L	—	—	—	—
K K	0.5	+/- 0.0	0.2	+/- 0.0
K L	—	—	—	—
Ca K	0.1	+/- 0.0	0.0	+/- 0.0
Ca L	—	—	—	—
Cr K	0.8	+/- 0.1	0.2	+/- 0.0
Cr L	—	—	—	—
Total	100.0		100.0	

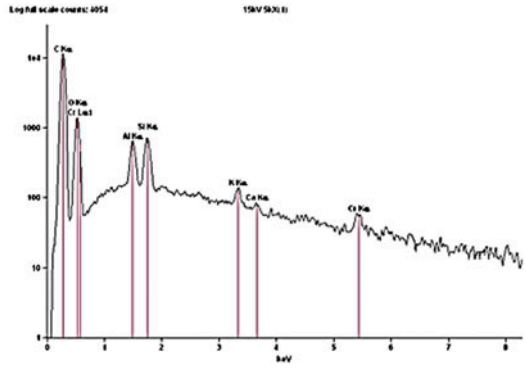

Fig. 4. Energy-dispersive spectra (EDX) of RGO.

are flat and larger than 500 nm in wideness. Due to the sonication the van der Waals interactions between GO layers is destroyed, and the existence of a large amount of oxygen-containing functional groups on the surface of GO nanosheets make single- or few-layer GO. The RGO nanosheets as shown in Fig. 8 are layer-structured, irregular, and folding. They are entangled with each other and lots of wrinkles. Corrugation and scrolling suggested the intrinsic nature of graphene, because the 2D structure would be thermodynamically stable via blending [29].

AFM is a powerful tool to measure the thickness of the samples. The typical AFM images of GO and RGO with line profile are indicated in Figs. 9 and 10. The 3D AFM images represent surface morphologies which are quite different. For GO, the typical roughness is about 21.7 nm, while for RGO the roughness is about 2.93 nm. GO is much thicker due the existence of epoxy, carboxyl, and hydroxyl groups on the both sides. There is more information in figures and tables. It is obvious that RGO nanosheets are fully exfoliated (Fig. 10). RGO AFM image reveals that the sheets display height variations. The results clearly illustrate that after MHR treatment GO has been reduced and has formed single or few layers of graphene.

3.2. Effect of solution pH

All experiments were done three times in order to check the reusability for RGO nanosheets adsorbent. The pH of the dye solution effects on the surface charge of the adsorbent, the degree of ionization of the materials and the dissociation of functional groups on the active sites of the adsorbent [30]. Therefore, it is one of the most important factors to study the adsorption property of an adsorbent. Fig. 11 shows the effect of the initial pH on the adsorption of BB41 onto RGO. It is found that increasing solution pH significantly increases the adsorption capacity in the pH range from 3 to 9.5 and the maximum removal of dye is at pH 9. The adsorption capacity correspondingly increases from 41.86 to 119.03 mg/g then decreases to 111.47 mg/g at pH 9.5. In particular, at pH ≥ 10 the color of the dye changes to red. Color and absorption

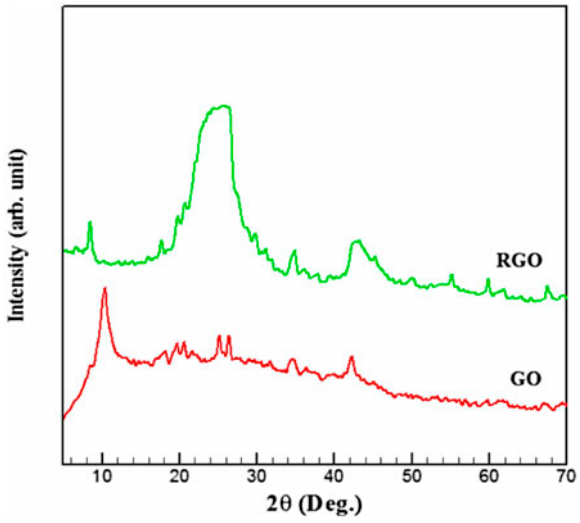

Fig. 5. XRD patterns of GO and rGO nanosheets.

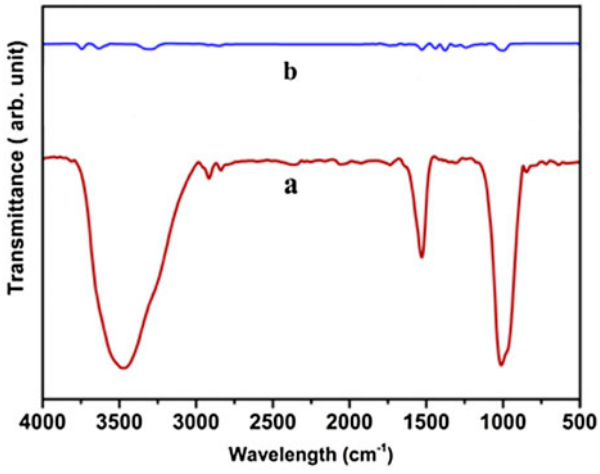

Fig. 6. FTIR spectrum of (a) GO and (b) RGO.

of the dye change with pH, which may attribute to the molecular structural variation of the dye at that pH range [31]. Also, the π–π interaction between the electron orbit perpendicular to graphene surface and BB41 containing electrons might be responsible for the adsorption of BB41 on RGO [32].

3.3. Effect of adsorbent dose

The effect of different adsorbent dosages on BB41 removal was carried out and the result for two initial BB41 concentrations (50 and 75 mg/L) are shown in Fig. 12. It can be seen the BB41 removal percentage increases by increasing graphene dose. The BB41 removal increases from 25 to 90% for an increase in adsorbent dose from 0.01 to 0.09 g/L and reaches on equilibrium value after 0.05 g of RGO. It is due to that increasing adsorbent dose serves to increase the surface area and the number of BB41 active sites for adsorption [33]. The BB41 adsorption capacity of RGO decreases by increasing RGO dosage (Fig. 12). The decrease in amount of BB41 adsorbed on to an adsorbent q_e (mg/g) with increasing RGO dose is due to that all active sites are entirely exposed and utilized at lower graphene dose and only part of active sites are exposed and occupied by BB41 at higher graphene dose. This is mainly attributed to non-saturation of the adsorption sites during the adsorption process [34]. At the same graphene dosage, higher BB41 concentration acquires a higher equilibrium adsorption capacity; this is because of that the larger BB41 concentration gradient increases the diffusion driving force of BB41 adsorbed by graphene [35,36]. When the RGO further increases after 0.05 g, there is no significant change in adsorption, thus 0.05 g of RGO adsorbent dose was chosen to study other parameters.

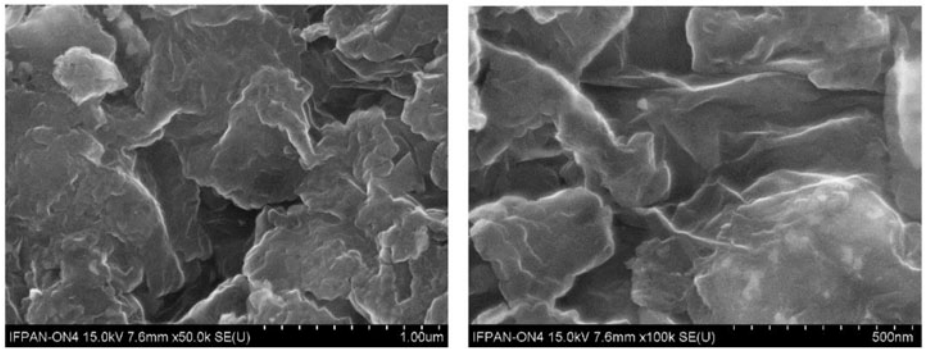

Fig. 7. SEM of GO.

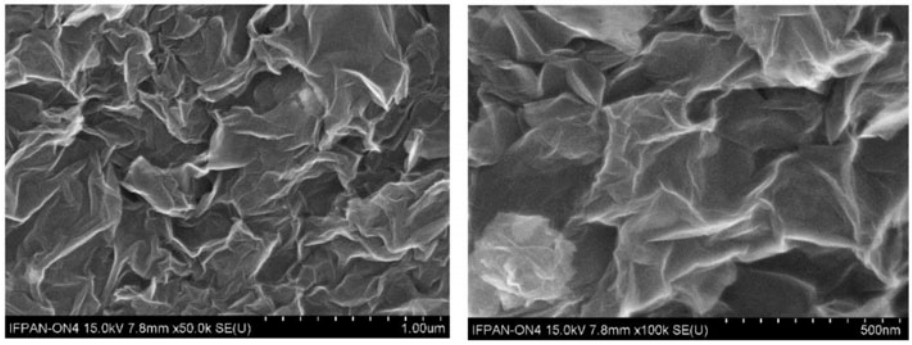

Fig. 8. SEM of RGO.

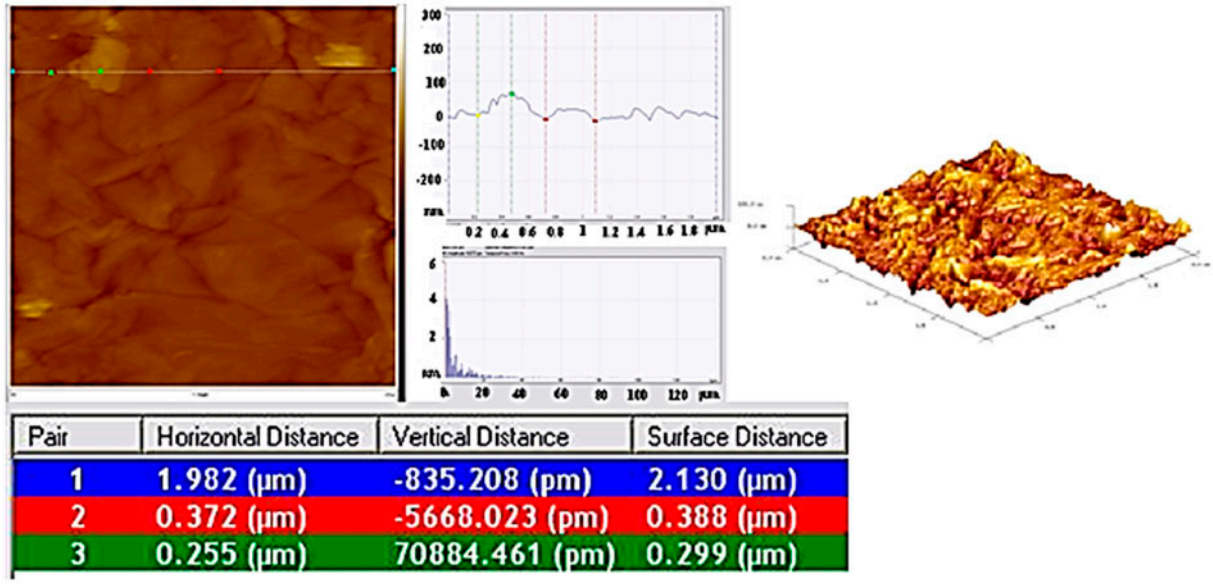

Fig. 9. AFM images of GO.

3.4. Effect of contact time

The effect of contact time on adsorption of BB41 onto RGO was studied at two initial BB41 concentrations (50 and 75 mg/L) for the adsorbent dose of 0.05 g which is shown in Fig. 13. It shows rapid adsorption of BB41 in the first 180 min and the amount of dye adsorbed at equilibrium increases from 96.48 to 143.59 mg/g with the increase in dye concentration from 50 to 75 mg/L. The rapid adsorption at the initial contact time is due to the accessibility of the negatively charged surface of RGO, which led to fast electrostatic adsorption of cationic BB41 from the solution. There are more available adsorption sites at lower dye concentration, while at higher concentrations the available site of adsorption is few and it takes long time to saturate. When the adsorption of the exterior surface reached saturation, the available sites are decreased and it is impossible the adsorbate particles diffuse deeper into the adsorbent structure [37].

3.5. Effect of initial dye concentration

The effect of initial concentration of BB41 adsorption on to RGO is presented in Fig. 14. Different concentrations (25, 50, 75, 100, and 125 mg/L) were used; the BB41 removal percentage decreased from 97.29 to 10.57% after 180 min as initial concentration increased. It is obvious that the adsorption of BB41 depends on the dye concentration. This could be attributed to the increase in driving force of concentration gradient, because the increase of dye concentration could

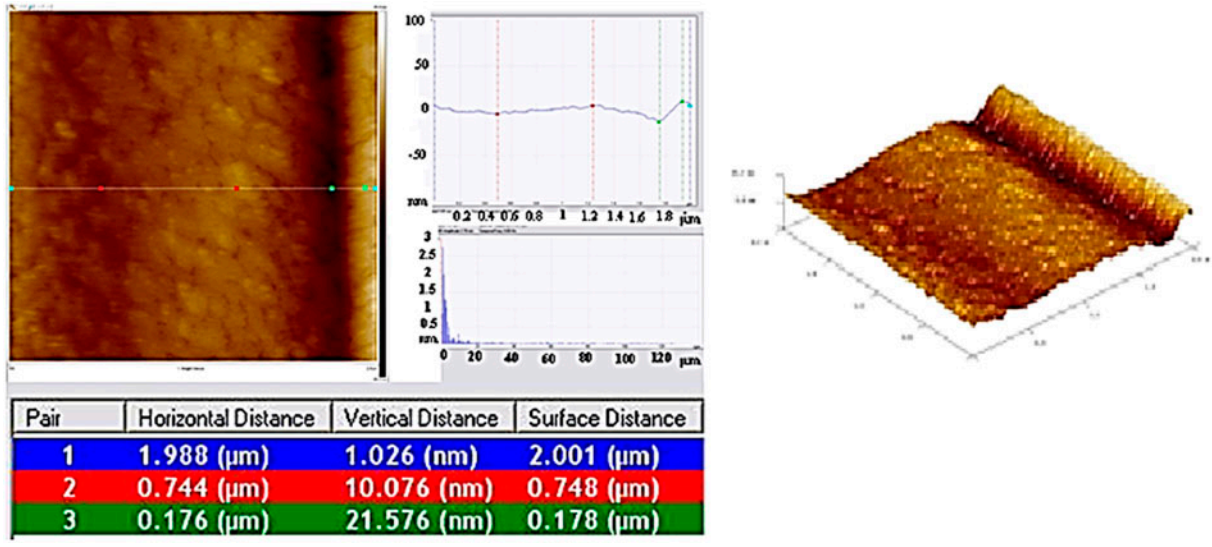

Fig. 10. AFM images of RGO.

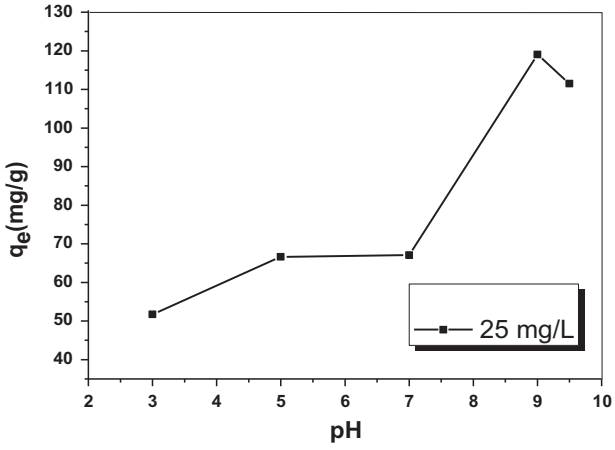

Fig. 11. Effect of pH on BB41 adsorption by RGO.

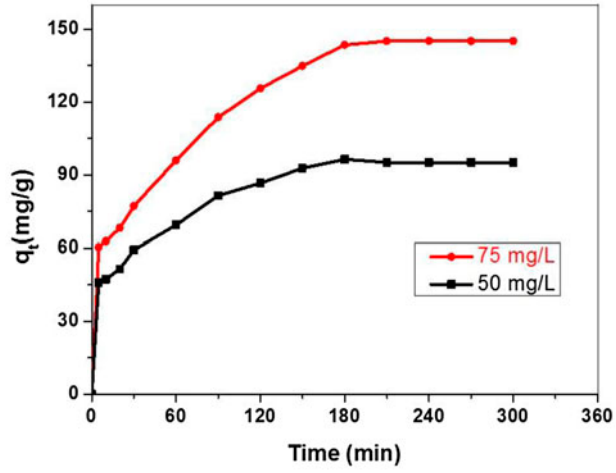

Fig. 13. Effect of contact time on BB41 adsorption by RGO.

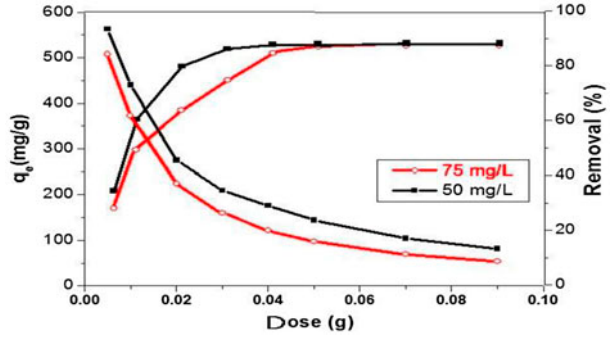

Fig. 12. Effect of RGO dose and adsorption capacity on BB41 removal for 50 and 75 mg/L dye concentration.

accelerate the diffusion of dye molecules onto the adsorbent, therefore at higher concentrations the available site of adsorption become fewer and consequently the dye ions take more time in order to reach the last available sites [30].

3.6. Adsorption isotherms

The adsorption isotherm represents the relationship between the adsorbed amount by a unit weight of solid adsorbent and the amount of adsorbate remained in the solution at equilibrium time [38]. Langmuir and Freundlich isotherms were used to describe the equilibrium adsorption. The Langmuir

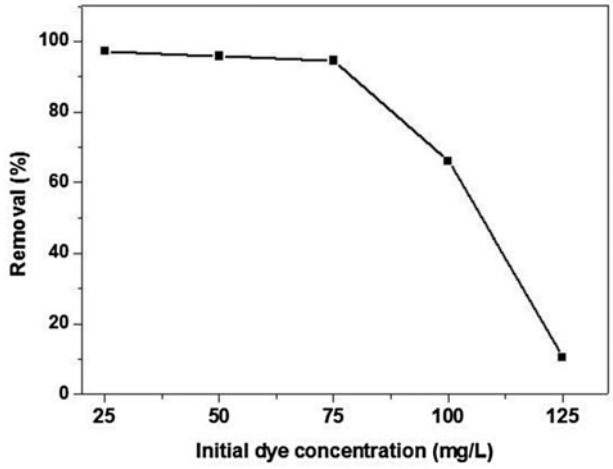

Fig. 14. Effect of initial dye concentration on BB41 adsorption by RGO.

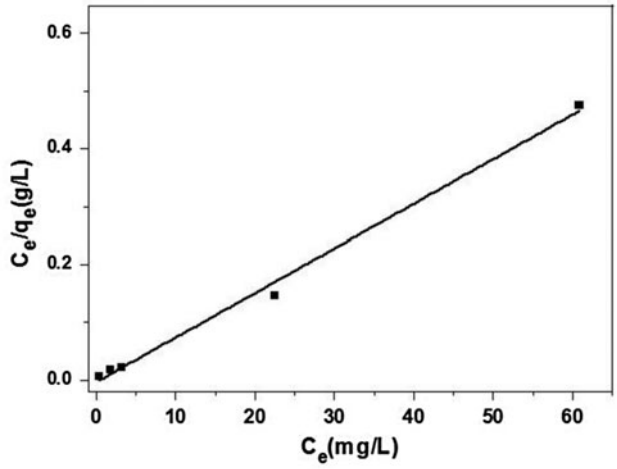

Fig. 15. Langmuir model for BB41 adsorption by RGO.

isotherm assumes that the adsorption occurs on a homogenous surface and there is no interaction between adsorbents in the plane of the surface [39]. The equation of the Langmuir isotherm is as follows:

$$\frac{C_e}{q_e} = \frac{C_e}{q_{max}} + \frac{1}{q_{max} k_L} \tag{3}$$

where C_e is the equilibrium concentration of the solution (mg/L), q_{max} is the maximum adsorption capacity (mg/g), k_L is a Langmuir constant related to the affinity of the binding sites and energy of adsorption (L/g). A straight line was obtained when C_e/q_e was plotted against C_e (Fig. 15), and q_{max} and k_L could be evaluated from the slope and intercept, respectively (Table 1).

The BB41 maximum adsorption capacity of RGO is 129.87 mg/g. The determination of R^2 coefficient of the Langmuir equation demonstrates that the adsorption of BB41 onto RGO follows the Langmuir's model. A dimensionless equilibrium parameter R_L is defined as follows [40]:

$$R_L = \frac{1}{1 + k_L C_0} \tag{4}$$

where k_L is the Langmuir constant (L/g) and C_0 is the highest initial dye concentration (mg/L). This parameter indicates the isotherm is unfavorable ($R_L > 1$), favorable ($R_L < 1$), linear ($R_L = 1$), or irreversible ($R_L = 0$) [41]. Table 1 shows R_L value between 0 and 1, which indicates the adsorption of BB41 onto RGO is favorable.

The Freundlich isotherm is an empirical equation based on sorption on heterogeneous surface through a multilayer adsorption mechanism [42]. The linearized form of the Freundlich equation is given as follows:

$$\ln q_e = \ln k_F + \frac{1}{n} \ln C_e \tag{5}$$

where k_F is a Freundlich constant related to adsorption capacity (L/g), $1/n$ is an empirical parameter related to adsorption intensity. A straight line is obtained when it is plotted against $\ln C_e$ (Fig. 16) and n and k_F could be evaluated from the slope and intercept, respectively (Table 1). According to the determined coefficients, the Langmuir model fits better than Freundlich model.

Table 1
Langmuir and Freundlich isotherms data

Temperature (K)	Langmuir				Freundlich		
	q_{max} (mg/g)	k_L (L/g)	R^2	R_L	$1/n$	k_F (L/g)	R^2
298	129.87	0.40	0.9948	0.024	0.1804	79.95	0.6356

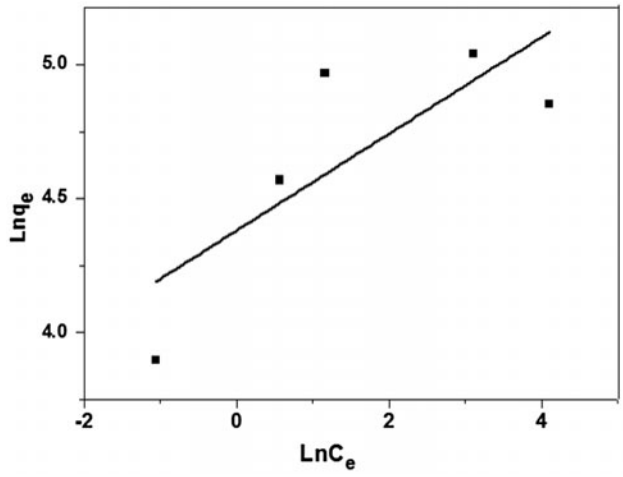

Fig. 16. Freundlich model for BB41 adsorption by RGO.

4. Conclusion

Graphene oxide was prepared using the Hummer method and reduced by MHR. The interlayer spacing was about 0.84 nm from XRD pattern. The FTIR spectra represented great effective deoxygenating of GO nanosheets via using MHR. The reduction was confirmed by SEM and AFM images and showed single or few layers of graphene.

RGO nanosheets have been utilized as the adsorbent for the removal of BB41dye from an aqueous solution at room temperature. It was found that by increasing solution pH from 3 to 9, the adsorption capacity significantly increased from 41.86 to 119.03 mg/g. The BB41 removal increased from 25 to 90% for an increase in adsorbent dose from 0.01 to 0.09 g/L. It is due to increase of the surface area and the number of BB41 active sites for adsorption. There was a rapid adsorption of BB41 in the first 180 min and the amount of dye adsorbed at equilibrium increases from 96.48 to 143.59 mg/g with the increase in dye concentration from 50 to 75 mg/L. The BB41 removal percentage decreased from 97.29 to 10.57% after 180 min as initial dye concentration increased from 25, 50, 75, 100, and 125 mg/L.

The Langmuir model was fitted to the data better than the Freundlich model. The results indicated that RGO can be employed as a low-cost alternative compared to other commercial adsorbents in the removal of dyes from wastewater. Also, the reduction method is convenient for mass production.

References

[1] C.H. Liu, J.S. Wu, H.C. Chiu, S.Y. Suen, K.H. Chu, Removal of anionic reactive dyes from water using anion exchange membranes as adsorbers, Water Res. 41 (2007) 1491–1500.
[2] K.M. Parida, S. Sahu, K.H. Reddy, P.C. Sahoo, A kinetic, thermodynamic, and mechanistic approach toward adsorption of methylene blue over water-washed manganese nodule leached residues, Ind. Eng. Chem. Res. 50 (2011) 843–848.
[3] Z. Aksu, Application of biosorption for the removal of organic pollutants: A review, Process Biochem. 40 (2005) 997–1026.
[4] H.-J. Hsing, P.-C. Chiang, E.-E. Chang, M.-Y. Chen, The decolorization and mineralization of Acid Orange 6 azo dye in aqueous solution by advanced oxidation processes: A comparative study, J. Hazard. Mater. 141 (2007) 8–16.
[5] K.P. Katuri, S.V. Mohan, S. Sridhar, B.R. Pati, P.N. Sarma, Laccase-membrane reactors for decolorization of an acid azo dye in aqueous phase: Process optimization, Water Res. 43 (2009) 3647–3658.
[6] L.V. Gonzalez-Gutierrez, E.M. Escamilla-Silva, Reactive red azo dye degradation in a UASB bioreactor: Mechanism and kinetics, Eng. Life Sci. 9 (2009) 311–316.
[7] Y. Safa, H.N. Bhatti, Kinetic and thermodynamic modeling for the removal of Direct Red-31 and Direct Orange-26 dyes from aqueous solutions by rice husk, Desalination 272 (2011) 313–322.
[8] Z. Belala, M. Jeguirim, M. Belhachemi, F. Addoun, G. Trouvé, Biosorption of basic dye from aqueous solutions by Date Stones and Palm-Trees Waste: Kinetic, equilibrium and thermodynamic studies, Desalination 271 (2011) 80–87.
[9] Y.H. Li, Q.J. Du, T.H. Liu, Y. Qi, P. Zhang, Z. Wang, Y. Xia, Preparation of activated carbon from *Enteromorpha prolifera* and its use on cationic red X-GRL removal, Appl. Surf. Sci. 257 (2011) 10621–10627.
[10] C.Y. Kuo, C.H. Wu, J.Y. Wu, Adsorption of direct dyes from aqueous solutions by carbon nanotubes: Determination of equilibrium, kinetics and thermodynamics parameters, J. Colloid Interface Sci. 327 (2008) 308–315.
[11] J.L. Gong, B. Wang, G.M. Zeng, C.P. Yang, C.G. Niu, Q.Y. Niu, W.J. Zhou, Y.J. Liang, Removal of cationic dyes from aqueous solution using magnetic multi-wall carbon nanotube nanocomposite as adsorbent, J. Hazard. Mater. 164 (2009) 1517–1522.
[12] A.K. Geim, K.S. Novoselov, The rise of graphene, Nat. Mater. 6 (2007) 183–191.
[13] S. Stankovich, R.D. Piner, S.T. Nguyen, R.S. Ruoff, Synthesis and exfoliation of isocyanate-treated graphene oxide nanoplatelets, Carbon 44 (2006) 3342–3347.
[14] S. Stankovich, D.A. Dikin, R.D. Piner, K.A. Kohlhaas, A. Kleinhammes, Y. Jia, Y. Wu, S.T. Neguyen, R.S. Rouff, Synthesis of graphene-based nanosheets via chemical reduction of exfoliated graphite oxide, Carbon 45 (2007) 1558–1565.
[15] C.Mm. Chen, Q.H. Yang, Y.G. Yang, W. Lv, Y.F. Wen, P.X. Hou, M.Z. Wang, H.M. Cheng, Self-assembled free-standing graphite oxide membrane, Adv. Mater. 21 (2009) 3007–3011.
[16] D.A. Dikin, S. Stankovich, E.J. Zimney, R.D. Piner, G.H.B. Dommett, G. Evmenenko, S.T. Nguyen, R.S. Ruoff, Preparation and characterization of graphene oxide paper, Nature 448 (2007) 457–460.

[17] S. Stankovich, D.A. Dikin, G.H.B. Dommett, K.M. Kohlhaas, E.J. Zimney, E.A. Stach, R.D. Piner, S.T. Nguyen, R.S. Ruoff, Graphene-based composite materials, Nature 442 (2006) 282–286.
[18] S. Park, J.H. An, I.W. Jung, R.D. Piner, S.J. An, X.S. Li, A. Velamakanni, R.S. Ruoff, Colloidal suspensions of highly reduced graphene oxide in a wide variety of organic solvents, Nano Lett. 9 (2009) 1593–1597.
[19] G.X. Wang, J. Yang, J. Park, X.L. Gou, B. Wang, H. Liu, J. Yao, Facile synthesis and characterization of graphene nanosheets, J. Phys. Chem. C 112 (2008) 8192–8195.
[20] H.-J. Shin, K.K. Kim, A. Benayad, S.-M. Yoon, H.K. Park, I.-S. Jung, M.H. Jin, H.-K. Jeong, J.M. Kim, J.-Y. Choi, Y.H. Lee, Efficient reduction of graphite oxide by sodium borohydride and its effect on electrical conductance, Adv. Funct. Mater. 19 (2009) 1987–1992.
[21] N. Li, M. Zheng, X. Chang, G. Ji, H. Lu, L. Xue, L. Pan, J. Cao, Preparation of magnetic $CoFe_2O_4$-functionalized graphene sheets via a facile hydrothermal method and their adsorption properties, J. Solid State Chem. 184 (2011) 953–958.
[22] G. Zhao, L. Jiang, Y. He, J. Li, H. Dong, X. Wang, W. Hu, Sulfonated graphene for persistent aromatic pollutant management, Adv. Mater. 23 (2011) 3959–3963.
[23] Y.H. Li, P. Zhang, Q. Du, X. Peng, T. Liu, Z. Wang, Y. Xia, W. Zhang, K. Wang, H. Zhu, D. Wu, Adsorption of fluoride from aqueous solution by graphene, J. Colloid Interface Sci. 363 (2011) 348–354.
[24] W.S. Hummers, R.E. Offeman, Preparation of graphitic oxide, J. Am. Chem. Soc. 80 (1958) 1339–1339.
[25] S. Kimiagar, N. Rashidi, E.E. Ghadim, Investigation of the effects of temperature and time on reduction of graphene oxide by microwave hydrothermal reactor, Bull. Mater. Sci. 38 (2015) 1699–1704.
[26] J.K. Lee, K.B. Smith, C.M. Hayner, H.H. Kung, Silicon nanoparticles–graphene paper composites for Li ion battery anodes, Chem. Commun. 46 (2010) 2025–2027.
[27] C. Fu, G. Zhao, H. Zhang, S. Li, Evaluation and characterization of reduced graphene oxide nanosheets as anode materials for lithium-ion batteries, Int. J. Electrochem. Sci. 8 (2013) 6269–6280.
[28] W. Gao, L.B. Alemany, L. Ci, P.M. Ajayan, New insights into the structure and reduction of graphite oxide, Nat. Chem. 1 (2009) 403–408.
[29] Z.L. Wang, D. Wu, Y. Huang, Z. Wu, L. Wang, X. Zhang, Facile, mild and fast thermal-decomposition reduction of graphene oxide in air and its application in high-performance lithium batteries, Chem. Commun. (Cambridge, UK) 48 (2012) 976–978.
[30] S. Dawood, T. Tushar K. Sen, Review on dye removal from its aqueous solution into alternative cost effective and non-conventional adsorbents, J. Chem. Proc. Eng. 1 (2014) 1–11.
[31] S. Debnath, A. Maity, K. Pillay, Impact of process parameters on removal of Congo red by graphene oxide from aqueous solution, J. Environ. Chem. Eng. 2 (2014) 260–272.
[32] X. Wan, B. Liu, Q. Lu, Q. Qu, Graphene-based materials: Fabrication and application for adsorption in analytical chemistry, J. Chromatogr. A 1362 (2014) 1–15.
[33] E.N. El Qada, S.J. Allen, G.M. Walker, Adsorption of basic dyes onto activated carbon Using microcolumns, Ind. Eng. Chem. Res. 45 (2006) 6044–6049.
[34] R. Han, W. Zou, Z. Zhang, J. Shi, J. Yang, Removal of copper(II) and lead(II) from aqueous solution by manganese oxide coated sand, J. Hazard. Mater. 137 (2006) 384–395.
[35] Y.H. Li, Q. Du, X. Wang, P. Zhang, D. Wang, Z. Wang, Y. Xia, Y.Z. Xia, Removal of lead from aqueous solution by activated carbon prepared from *Enteromorpha prolifera* by zinc chloride activation, J. Hazard. Mater. 183 (2010) 583–589.
[36] T. Liu, Y. Li, Q. Du, J. Sun, Y. Jiao, G. Yang, et al., Adsorption of methylene blue from aqueous solution by graphene, Colloids Surf., B 90 (2012) 197–203.
[37] Y.H. Li, T. Liu, Q. Du, J. Sun, Y. Xia, Z. Wang, W. Zhang, K. Wang, H. Zhu, D. Wu, Adsorption of cationic red X-GRL from aqueous solutions by graphene: Equilibrium, kinetics and thermodynamics study, Chem. Biochem. Eng. Q 25 (2011) 483–491.
[38] Z. Hu, H. Chen, F. Ji, Removal of Congo Red from aqueous solution by cattail root, J. Hazard. Mater. 173 (2010) 292–297.
[39] I. Langmuir, The constitution and fundamental properties of solids and liquids. Part I. Solids, J. Am. Chem. Soc. 38 (1916) 2221–2295.
[40] T.W. Weber, R.K. Chakravorti, Pore and solid diffusion models for fixed-bed adsorbers, AIChE J. 20 (1974) 228–238.
[41] M. Chen, Y. Chen, G.W. Diao, Adsorption kinetics and thermodynamics of methylene blue onto p-tert-butyl-calix[4,6,8]arene-bonded silica gel, J. Chem. Eng. Data 55 (2010) 5109–5116.
[42] H.M.F. Freundlich, Over the adsorption in solution, J. Phys. Chem. 57 (1906) 385–470.